

Adsorption Behavior and Corrosion Inhibition Mechanism of Three Amino Acids on Mild Steel in 3.5% NaCl Solution: Electrochemical and Computational Studies

Dong Han¹, Jiarun Li², Ning Wang², Kai Wan^{1,*}

¹ Gaomi Campus of Qingdao University of Science and Technology, Gaomi 261500, Shandong, PR China.

² Key Laboratory of Marine Environmental Corrosion and Bio-fouling, Institute of Oceanology, Chinese Academy of Sciences, Qingdao 266071, Shandong, PR China.

*E-mail: wank@qust.edu.cn

Received: 1 June 2020 / Accepted: 29 July 2020 / Published: 31 August 2020

The adsorption behavior and corrosion inhibition mechanism of three amino acids have been studied by using weight loss, electrochemical test, scanning electron microscope, quantum chemical calculation and molecular dynamics simulation techniques. Gravimetric and electrochemical results showed the inhibition efficiencies both increased with the increasing L-arginine and L-lysine concentration from 1.0 g•L⁻¹ to 10.0 g•L⁻¹, the maximum inhibition efficiency 74.1% and 69.1% was obtained, respectively. However, the inhibition efficiency changed slightly with the increasing concentration of L-histidine. The adsorption behaviors of three amino acids obeyed the Langmuir isotherm and more details were given by theoretical calculation.

Keywords: Neutral inhibition, Mild steel, Amino acids, Weight loss, EIS, Modelling study

1. INTRODUCTION

Mild Steel has been widely used and played an important role in construction material such as petrochemical engineering, food and power industry due to its popular price, excellent welding performance and mechanical strength[1-4]. And nowadays, mild steel is being increasingly used in marine constructions. However, it invariably exposes in seawater and suffers from severe corrosion problem because of the existence of large quantities of aggressive substance such as chloride ion, sulfate ion and oxygen. One of the most important methods to hinder the corrosion and minimize the failure of mild steel is the usage of effective corrosion inorganic or organic inhibitors[5-8]. Unfortunately, almost all of the inorganic inhibitors have been prohibited application owing to their physiological and

biochemical toxicity to humans and creatures[9,10]. On account of this, Organic corrosion inhibitors have been attached much importance by recent research[11-14].

The effectiveness of organic corrosion inhibitors related to their molecule structures including chemical composition, charge density and active sites has been reported by many of the researchers[15,16]. Such compounds usually have polar atoms or groups like nitrogen, oxygen, sulfur, phosphorus atoms and π electron conjugated groups. These functional groups can donate their lone pair electrons to metal atoms and make interaction with coordinate covalent bonds. In addition, they sometimes adsorbed on the metal surface through electrostatic adsorption[17,18].

Even so, there is still a serious problem that some of the organic corrosion inhibitors with phosphorus atoms or others are confirmed toxic to the environment[19]. Based on the environmentally friendly consideration, several kinds of compounds such as chitosan[20-22,9], cellulose[23], amino acids[8,24,25], natural plant extractive[26-29] are accord with the demand of reducing environmental damage and recycling of materials. Our previous work mainly studied the enhanced corrosion inhibition properties of carboxymethyl hydroxypropyl chitosan for mild steel in 1.0 M HCl solution[30]. Amino acids which contain both carboxyl and amino groups also acted as corrosion inhibitors recently with low cost and non-toxic to the organism, and the corrosion inhibition performances have been studied by many researchers as well[31-33]. To the best of our knowledge, however, the corrosion inhibition medium was concentrated on acid medium, there is a lack of study on corrosion inhibition behavior and mechanism of amino acids in neutral medium. Moreover, quantum chemistry study and molecular dynamics simulation as powerful theoretical tools aiming at establishing the relationship between experimental and theoretical consequences were applied. They are utilized to study the reaction mechanism based on the molecule level[34-36].

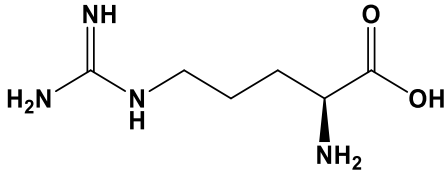
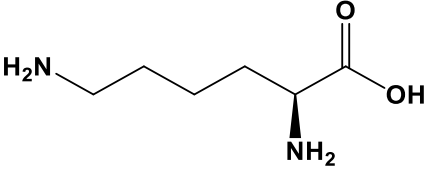
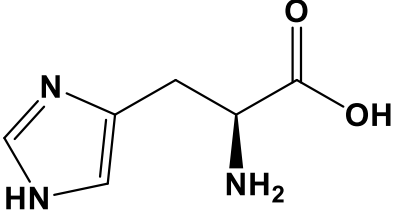
For the green chemistry and corrosion inhibition medium purpose, our current work mainly focused on studying the corrosion inhibition performances and mechanism of three amino acids L-arginine (L-Arg), L-lysine (L-Lys) and L-histidine (L-His) by using weight loss measurements, potentiodynamic polarization and electrochemical impedance spectroscopy (EIS), meanwhile, putting forward and detailing the adsorption mechanism. Scanning electron microscopy (SEM) was also used to observe the surface morphology. In addition, adsorption behavior in molecule level was studied by using theoretical and computational research.

2. EXPERIMENTAL

2.1 Materials

All the used amino acids (L-Arg, L-Lys, L-His) of analytical grade were purchased from Sinopharm Chemical Reagent CO., Ltd. The names, chemical structures, molecule weight and isoelectric points (pI) of amino acids were shown in Table 1. The working electrodes were made of mild steel composed in wt. %, C: 0.17, Mn: 0.46, Si: 0.3, S: 0.050, P: 0.045.

Table 1. The names, structures, molecular weights and isoelectric points of three amino acids.

Name	Structure	Molecular weight	Isoelectric point
L-arginine		174.20	9.74
L-lysine		146.19	10.76
L-histidine		155.00	7.59

2.2. Preparation of electrode system

Electrochemical test mild steel specimens were cut into 1 cm² of the surface area exposed to electrolyte. Test panels (50 mm × 25 mm × 3 mm) were used for weight loss measurements. They were polished sequentially with 400 grit, 800 grit, 1200 grit, 1500 grit and 2000 grit emery papers and then degreased in acetone and ethanol prior to immersing test solution for electrochemical measurements. The test system consisted of a typical three-electrode configuration and the mild steel was used as a working electrode (A=1 cm²). The mild steel was encapsulated in epoxy resin in polyvinyl chloride pipe with electrical contact connected with a copper wire into metal surface. The standard calomel electrode (SCE) and platinum electrode were served as reference and counter electrode (CE, A=4 cm²), respectively.

2.3. Test solutions

AR grade NaCl was used to prepare the aggressive solution. The test solution was prepared using deionized water with 3.5 wt.% NaCl. The concentration of corrosion inhibitor was ranged from 0.1 g•L⁻¹ to 10 g•L⁻¹. All of the inhibitors could be completely dissolved in the solution.

2.4. Methods

All the experiments were operated in atmospheric pressure and 25 ± 1 °C. All of the working electrodes were immersed in test solution for 3 h before measurements. An electrochemical workstation (PARSTAT 2273, Princeton, Inc.) was employed for obtaining the electrochemical data of corrosion inhibitors.

2.4.1. Weight loss experiments

Test coupons were washed out using deionized water, rinsed with ethanol and acetone, and then dried at room temperature. Four parallel samples were completely immersed in 2 L glass beaker for 7 days containing aggressive solutions with and without corrosion inhibitor of different concentrations after weighting accurately. After immersion time, the samples were taken out, washed with a brush and cleaned by 1:1 v/v H₂O and concentrated hydrochloric acid + 3.5 g•L⁻¹ hexamethylene tetramine for 10 min at 25 °C, dried and accurately weighed. The average mass values of four samples were calculated as the results.

2.4.2. Electrochemical measurements

Potentiodynamic polarization curves were obtained by automatically changing the electrode potential from -250 mV to +250 mV vs OCP at a constant sweep rate of 0.5 mV/s. Electrochemical impedance spectroscopy measurements at free corrosion potential were performed at different concentrations after the working electrodes came to a stable state. The scanning frequency was ranged from 100 kHz to 10 mHz with a voltage perturbation of 10 mV. The electrochemical data were analyzed by using the software ZSimpWin.

2.4.3. SEM observation

The metallic surfaces of samples were observed before and after immersion in 3.5 wt.% NaCl with different concentrations of corrosion inhibitors by using scanning electron microscopy (JSF-6700F).

2.4.4. Quantum chemical calculations and molecular dynamics (MD) simulations

The quantum chemical calculations were performed with Gaussian 09W software by using density functional theory (DFT) B3LYP method with 6-31G (d, p) to optimize the geometric configuration of corrosion inhibitor molecules[37]. Several parameters such as the highest occupied atomic orbital (E_{HOMO}), the lowest unoccupied molecular orbitals (E_{LUMO}), energy gap (ΔE : $\Delta E = E_{\text{LUMO}} - E_{\text{HOMO}}$), dipole moment (μ), the ionization potential (I), the electron affinity (A), the electronegativity (χ), the global hardness (γ) and the fraction of electron transferred (ΔN) were calculated. The relevant algorithm was listed as follows using the Koopmans' theorem[38,39]:

$$I = -E_{\text{HOMO}} \quad (1)$$

$$A = -E_{\text{LUMO}} \quad (2)$$

$$\chi = \frac{I+A}{2} \quad (3)$$

$$\gamma = \frac{I-A}{2} \quad (4)$$

$$\Delta N = \frac{\chi_{\text{Fe}} - \chi_{\text{inh}}}{2(\gamma_{\text{Fe}} + \gamma_{\text{inh}})} \quad (5)$$

Where χ_{Fe} and χ_{inh} represented the electronegativity of iron atom and inhibitor molecule, γ_{Fe} and γ_{inh} represented the hardness of iron atom and inhibitor molecule, respectively. In most cases, the value of χ_{Fe} was 7.0 and γ_{Fe} was 0[40].

The Fukui function was also used to select which atom was the most likely reaction center for instance nucleophilic or electrophilic attack. The correlative expressions using a scheme of finite difference approximations were listed as follows:

$$f_k^+ = P_k(N+1) - P_k(N) \quad (6)$$

$$f_k^- = P_k(N) - P_k(N-1) \quad (7)$$

where $P_k(N+1)$, $P_k(N)$, and $P_k(N-1)$ were the natural population, and f_k^+ and f_k^- were the values of Fukui function for three amino acids.

The MD simulations of the interactions between Fe surface (110) and corrosion inhibitor molecules were performed by using Materials Studio 8.0 (Accelrys Inc.). Before simulation, we first optimized the Fe cell and cleaved its surface along (110) plane, and then created a box composed of a Fe slab and a vacuum layer with the size of 14.89Å×9.93Å×33.11Å. The Fe (110) plane was enlarged to a supercell of 6×6. The simulation was performed with the total time step of 1000 ps and a step time of 1.0 fs under 298 K by using compass force field and discover module.

3. RESULTS AND DISCUSSION

3.1. Weight loss experiments

The corrosion inhibition properties of three amino acids in 3.5 wt.% NaCl solution in different molality for 7 days at 25 °C were performed by weight loss experiments. The relationship among corrosion rate (v , $\text{mg}\cdot\text{cm}^{-2}\cdot\text{d}^{-1}$), the inhibition efficiency (η , %) and the corrosion inhibition concentration (c , $\text{g}\cdot\text{L}^{-1}$) was shown in Fig. 1. The relevant data were listed in Table 2. The corrosion rate and the inhibition efficiency were calculated by the following equations[41]:

$$v = \frac{W-W'}{ST} \quad (8)$$

$$\eta = \frac{v-v'}{v} \times 100 \quad (9)$$

Where the W and W' were the weight of the specimens in the absence and presence of amino acids. S (cm^2) was total surface test area of the specimens and T was the immersion time (7 d). v and v' were the corrosion rate without and with inhibition, respectively.

From Table 2 and Fig. 1, it could be seen that the corrosion rate without inhibitor was 3.531 $\text{mg}\cdot\text{cm}^{-2}\cdot\text{d}^{-1}$ and decreased much in the presence of inhibitor. While in the presence of L-Arg and L-Lys, the corrosion rate decreased with the increasing inhibitor concentration from 0.1 $\text{g}\cdot\text{L}^{-1}$ to 3.0 $\text{g}\cdot\text{L}^{-1}$ owing to the increase of adsorption on the metal surface, and then, the corrosion rate changed very little with the increasing concentration from 3.0 $\text{g}\cdot\text{L}^{-1}$ to 10.0 $\text{g}\cdot\text{L}^{-1}$. This is because the maximum adsorption had been obtained at this concentration range. However, the corrosion rate of L-His decreased with the concentration from 0.1 $\text{g}\cdot\text{L}^{-1}$ to 0.5 $\text{g}\cdot\text{L}^{-1}$, meanwhile, the corrosion rate changed a little with the increasing concentration from 0.5 $\text{g}\cdot\text{L}^{-1}$ to 10.0 $\text{g}\cdot\text{L}^{-1}$, indicating that the adsorption capacity reached the maximum at the concentration of about 0.5 $\text{g}\cdot\text{L}^{-1}$.

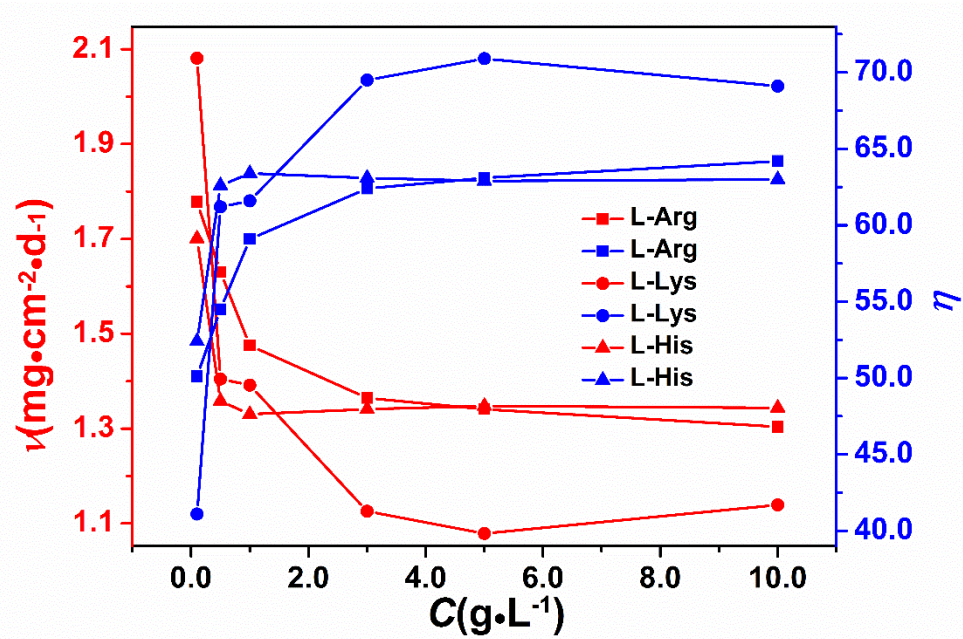


Figure 1. Relationship among corrosion rates, inhibition efficiencies and concentrations of three amino acids in 3.5% NaCl solution at 25 °C.

Table 2. Corrosion parameters obtained from weight loss measurements for mild steel in 3.5% NaCl solution in the absence and presence of corrosion inhibitors of various concentrations at 25 °C after 7 d immersion period.

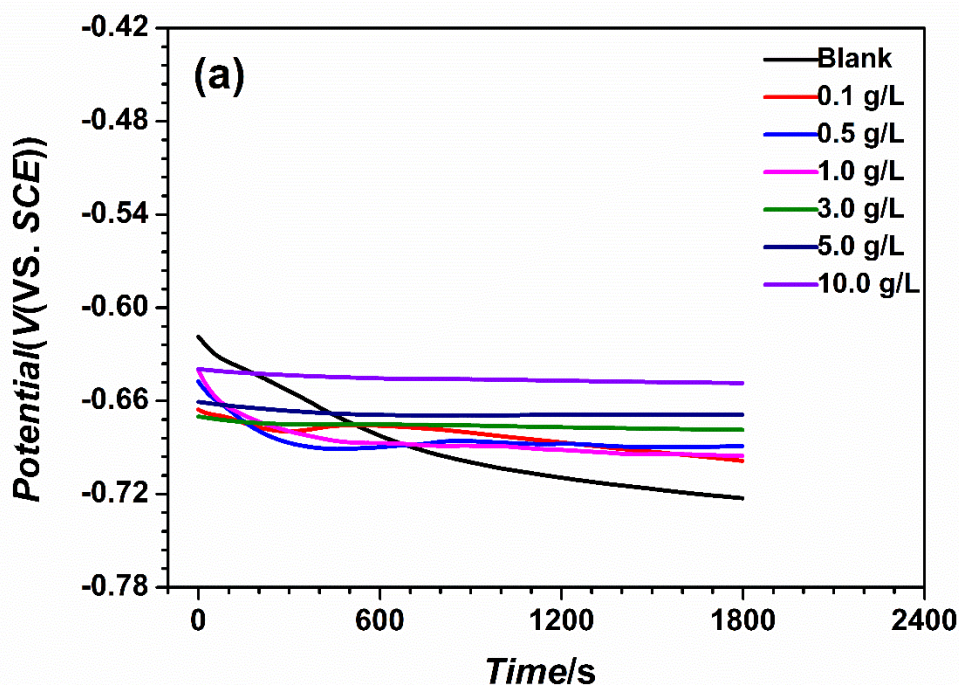
Inhibitor	Concentration (g·L ⁻¹)	v (mg·cm ⁻² ·d ⁻¹)	θ	η (%)
Blank	—	3.531	—	—
L-Arg	0.1	1.762	0.501	50.1
	0.5	1.607	0.545	54.5
	1.0	1.444	0.591	59.1
	3.0	1.328	0.624	62.4
	5.0	1.303	0.631	63.1
	10.0	1.264	0.642	64.2
L-Lys	0.1	2.080	0.411	41.1
	0.5	1.370	0.612	61.2
	1.0	1.356	0.616	61.6
	3.0	1.077	0.695	69.5
	5.0	1.028	0.709	70.9
	10.0	1.091	0.691	69.1
L-His	0.1	1.681	0.524	52.4
	0.5	1.321	0.626	62.6
	1.0	1.292	0.634	63.4
	3.0	1.303	0.631	63.1
	5.0	1.310	0.629	62.9
	10.0	1.306	0.63	63

3.2. Electrochemical measurements

3.2.1. Open circuit potential measurements (OCP)

After immersing in the test solution for 3 h to achieve a relatively stable state, the OCP values of the samples during the next 0.5 h immersion time were measured in the test solution. The relationship between the potential and the immersion time was shown in Fig. 2. In the solution without inhibitor, the corrosion potential decreased during immersion time at the potential of -722.6 mV, and at the concentration $10.0 \text{ g}\cdot\text{L}^{-1}$, this value was -648.5 mV for L-Arg, -650.9 mV for L-lys and -729.5 mV for L-His, in the same medium, respectively. The addition of three amino acids caused a potential change less than 80 mV. According to the Refs [42,43], a compound could act as a mixed-type inhibitor if the change in OCP value was less than 85 mV. Accordingly, these amino acids were defined as mixed-type inhibitors.

The OCP values in the presence of inhibitors shifted toward positive or negative direction from that of blank sample. In Figs. 2(a) and 2(b), the values increased with the increasing concentration owing to the greater inhibitor concentrations. Whereas in Fig. 2(c), the OCP values of L-His solution decreased, and then, with the increasing concentration of corrosion inhibitor, the values increased slightly, which could be interpreted that the reaction mechanism in the anode and cathode reaction was not changed.



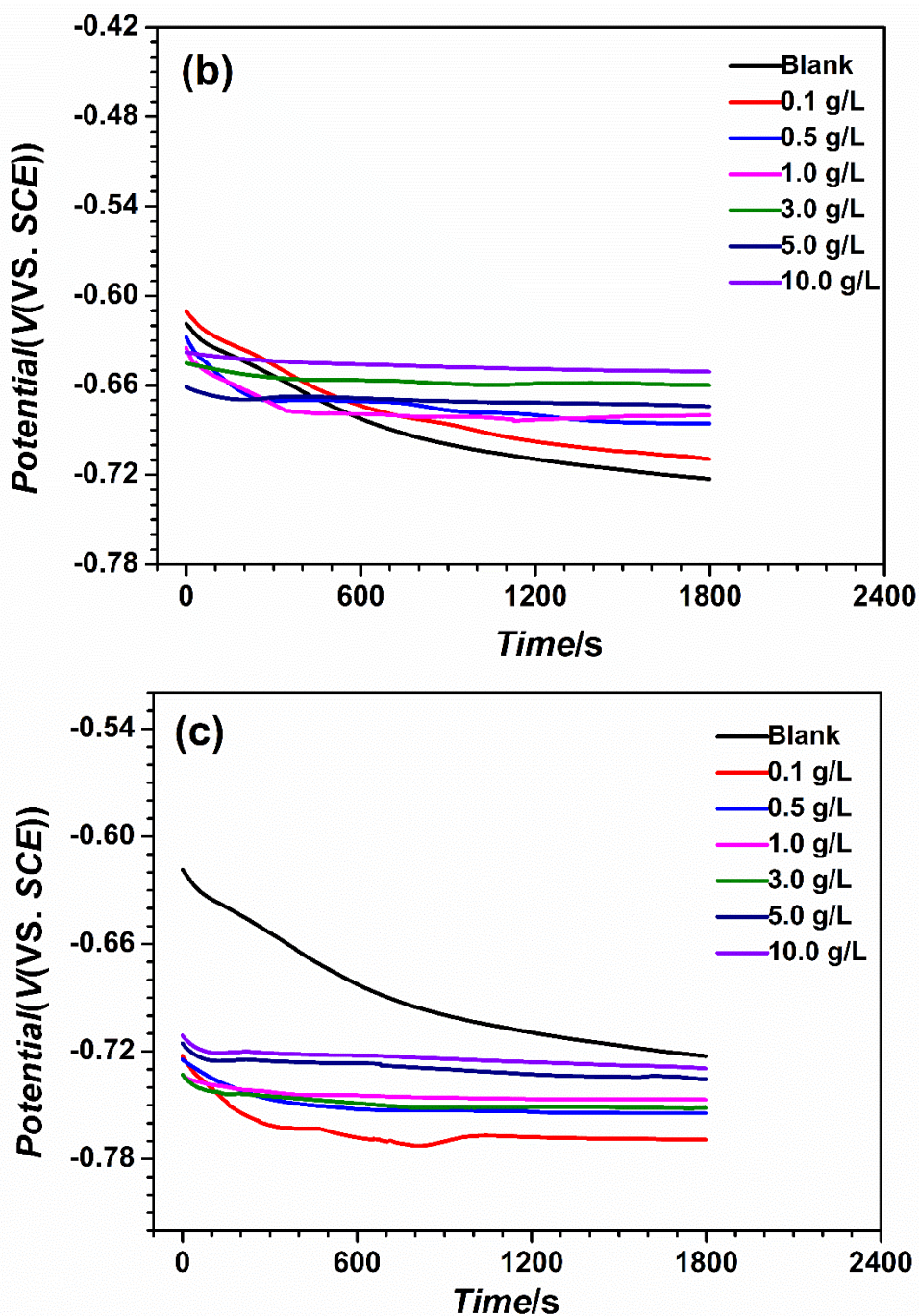


Figure 2. Open circuit potentials of (a) L-Arg (b) L-Lys and L-His (c) during immersion for mild steel in 3.5% NaCl solution at 25 °C.

An increasing or decreasing OCP value shows the physical or chemical change process. A relatively stable OCP value implies an equilibrium state among the advance of corrosion, absorption and desorption process and the deposit of corrosion products[44,45]. For the blank sample, the OCP values had a sustained downward trend, while the samples in the presence of inhibitor had two distinct stages during the testing time. In L-Arg and L-Lys cases, the values decreased continuously with the increasing immersion time at the relative low concentrations ($0.1 \text{ g}\cdot\text{L}^{-1}$, $0.5 \text{ g}\cdot\text{L}^{-1}$ and $1.0 \text{ g}\cdot\text{L}^{-1}$) during the first immersion time of 400-500 s, and as the reaction proceeded, they tended to the stable potentials for the following immersion time. This was an equilibrium state among the advance of corrosion, absorption

and desorption process and the deposit of corrosion products[44]. Meanwhile, a nearly constant potential reading for the inhibitors at relative high concentrations ($3.0 \text{ g}\cdot\text{L}^{-1}$, $5.0 \text{ g}\cdot\text{L}^{-1}$ and $10.0 \text{ g}\cdot\text{L}^{-1}$) during the immersion time, which suggested that the corrosion inhibition system had reached a stable state before the testing time. For the samples with L-His, these values were independent of inhibitor concentration in the range of $0.5\text{-}10.0 \text{ g}\cdot\text{L}^{-1}$. This could be attributed to a maximum adsorption in the $0.5 \text{ g}\cdot\text{L}^{-1}$ solution, the desorption and adsorption of inhibitors has reach the equilibrium.

3.2.2. Potentiodynamic polarization

Tafel plot analysis was used to study and compare the relative corrosion protection performances of the bare and PANI-coated films synthesized on MS in different ILs medium and were examined in a simulated marine environment in a 3.5% NaCl solution.

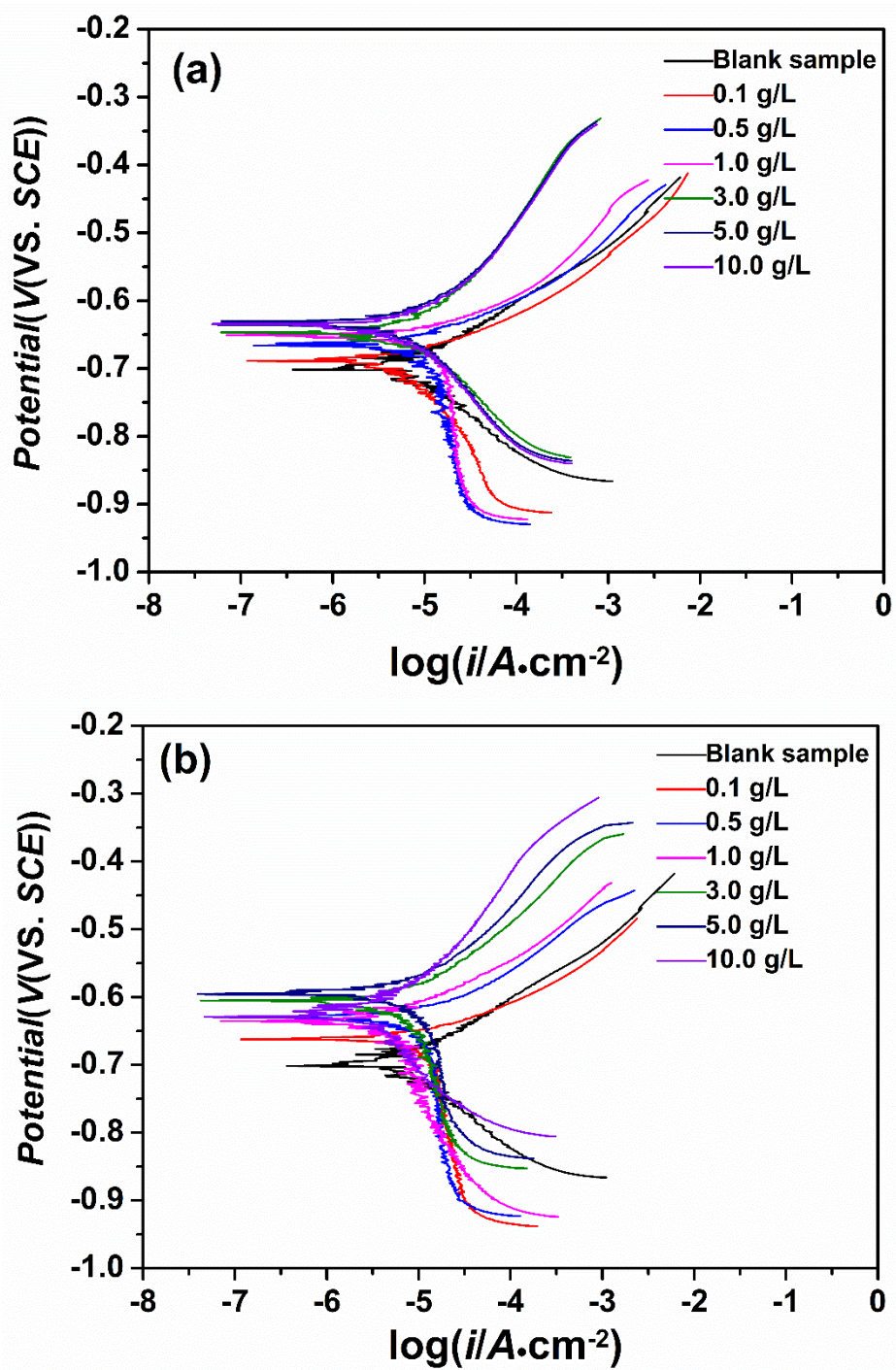
Fig. 3 showed the potentiodynamic polarization curves of carbon steel in 3.5 wt.% NaCl solution in the absence and presence of different concentrations of three amino acids at 298 K, respectively. Obviously, the addition of three inhibitors caused lower corrosion rate and corrosion current densities than the blank sample. In Fig. 3(a), it showed that the addition of L-Arg with the concentration $0.1\text{-}1.0 \text{ g}\cdot\text{L}^{-1}$ caused a sharp decrease in the cathodic region. The same phenomenon was also visible in Fig. 3(b) with the concentration $0.1\text{-}5.0 \text{ g}\cdot\text{L}^{-1}$ of L-Lys. This behavior was attributed to the suppressed cathodic oxygen diffusion reaction, which was under cathodic control. The addition of L-Arg with the concentration $3.0\text{-}10.0 \text{ g}\cdot\text{L}^{-1}$ and L-Lys $10.0 \text{ g}\cdot\text{L}^{-1}$ showed that both anodic and cathodic processes seemed to approximately be equal, which could be interpreted as the increasing anodic inhibiting effect with the increasing inhibitor concentration[46]. From Fig. 3(c), it suggested that the addition of L-His also reduced the anodic and cathodic reactions, in addition, the inhibition mechanism did not change with the increasing concentration. All electrodes in the presence of inhibitors represented a cathodic region of Tafel behavior [41], whereas, there was not a remarkable change in the anodic region. Accordingly, the corresponding kinetic parameters of polarization including corrosion current density (i_{corr}), anodic slope (β_a) and cathodic slope (β_c) were determined by using extrapolation method. The surface coverage (θ) and corrosion inhibition efficiency (η) were calculated by the equations below[47]:

$$\theta = \frac{i_{\text{corr}} - i'_{\text{corr}}}{i_{\text{corr}}} \quad (8)$$

$$\eta = \frac{i_{\text{corr}} - i'_{\text{corr}}}{i_{\text{corr}}} \times 100 \quad (9)$$

Where i_{corr} and i'_{corr} were the corrosion current density in the absence and presence of inhibited specimens. All the data were displayed in the Table 2.

According to the results in Fig. 3 and Table 2, it was obvious that both the anodic and cathodic current density decreased after the addition of the inhibitors. Iron dissolution in anodic region and oxygen diffusion in cathodic region would be suppressed by adding of the inhibitors. The parallel anodic Tafel lines indicated the anodic reaction mechanism was not modified after the addition of inhibitors, implying that the inhibitor molecules were just adsorbed on the metallic surface and protected the metal from corrosion[48,49].



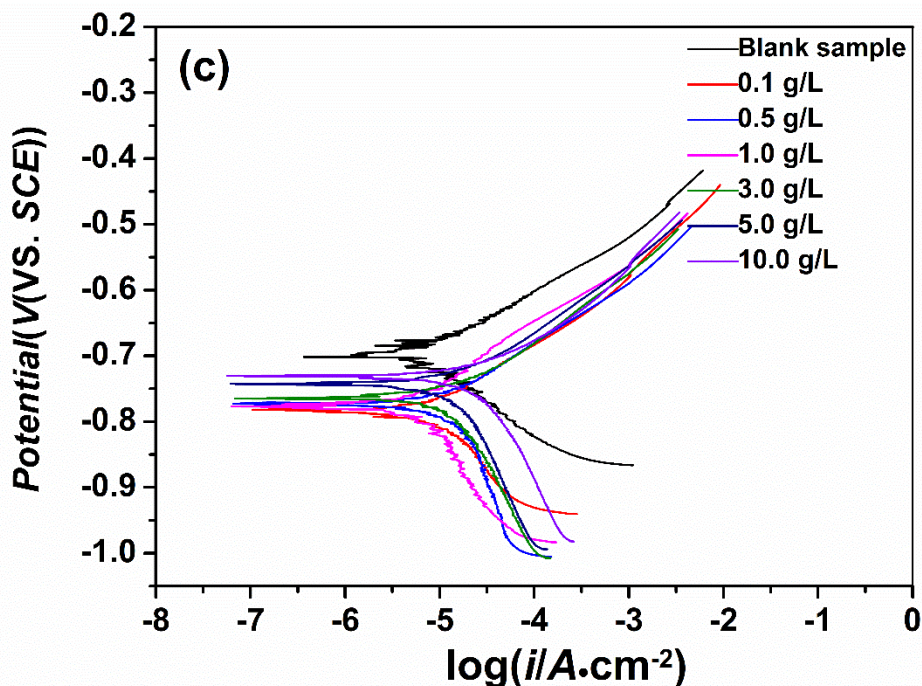


Figure 3. Potentiodynamic polarization curves of mild steel electrodes in presence of amino acids with various concentrations at 25 °C in 3.5% NaCl solution. (a) L-Arg (b) L-Lys (c) L-His

From Table 3, it was also clear that the inhibition efficiency (η) increased as the inhibitor concentration increased from 0.1 g·L⁻¹ to 1.0 g·L⁻¹ for the L-Arg and L-Lys due to the increasing number of active sites and adsorption amount, and then, this value was approximate at the concentration range of 3.0-10.0 g·L⁻¹, which was interpreted that adsorption is saturated on the metallic surface at these concentrations. The maximum values were 69.1% and 74.1%, respectively. In contrary to the L-Arg and L-Lys, there was no specific trend in the shift of inhibition efficiency for the L-His (0.5-10.0 g·L⁻¹), implying that no more adsorption occurred with the increasing concentration. The maximum inhibition efficiency value was 65.4%, slightly below those of L-Arg and L-Lys.

Table 3. Potentiodynamic polarization parameters for the corrosion of mild steel in 3.5% NaCl solution containing various concentrations of amino acids at 25 °C.

Inhibitor	C (g·L ⁻¹)	E_{corr} (mV VS SCE)	i_{corr} ($\mu\text{A}\cdot\text{cm}^{-2}$)	β_a (mV·dec ⁻¹)	β_c (mV·dec ⁻¹)	θ	η (%)
Blank	—	-723	6.073	91	-121	—	—
L-Arg	0.1	-699	2.875	75	-138	0.527	52.7
	0.5	-689	2.532	72	-257	0.583	58.3
	1.0	-695	2.387	71	-268	0.607	60.7
	3.0	-679	2.110	80	-134	0.653	65.3
	5.0	-669	2.083	79	-148	0.657	65.7
	10.0	-648	1.931	82	-139	0.682	68.2
L-Lys	0.1	-709	3.610	64	-231	0.404	40.4
	0.5	-686	2.141	63	-257	0.648	64.8
	1.0	-680	2.131	61	-229	0.649	64.9

L-His	3.0	-660	1.731	74	-271	0.715	71.5
	5.0	-674	1.652	77	-271	0.728	72.8
	10.0	-651	1.707	92	-143	0.719	71.9
	0.1	-769	2.826	87	-167	0.515	51.5
	0.5	-754	2.198	82	-213	0.638	63.8
	1.0	-747	2.135	86	-195	0.649	64.9
	3.0	-751	2.186	80	-193	0.640	64.0
	5.0	-735	2.143	80	-201	0.648	64.8
	10.0	-729	2.120	79	-198	0.651	65.1

3.2.3. Electrochemical impedance spectroscopy

Nyquist diagrams of carbon steel in 3.5 wt% NaCl solution in the presence of L-Arg, L-Lys and L-His with various electrochemical characteristics were presented in Figs. 4(a)-4(c), respectively. In Fig. 4, the impedance plots of blank sample composed of only a single capacitive loop, the diameter was minimal of capacitive loops. In the presence of L-Arg in the solution with the concentration of 0.1-1.0 $\text{g}\cdot\text{L}^{-1}$, a capacitive loop in the high frequency was also observed in the Fig. 4(a), which was ascribed to the charge transfer reaction at the electrode/electrolyte interface. The size of loops increased with increasing concentration, indicating the corrosion inhibition effect on the work electrode surface. However, in the presence of L-Arg with the concentrations of 3.0-10.0 $\text{g}\cdot\text{L}^{-1}$, two loops at high and low frequencies were seen in the Fig 4(a). In accordance with L-Arg, the same impedance plots of sample with the L-Lys concentration of 10.0 $\text{g}\cdot\text{L}^{-1}$ occurred in Fig.4(b). In Figs. 4(b) and 4(c), except for L-Lys with 10.0 $\text{g}\cdot\text{L}^{-1}$, all impedance plots were comprised of only one capacitive loop. In addition, the size of semicircles increased with the increasing concentrations in Fig. 4(b), whereas, there was no definite trend of impedance plots in the Fig. 4(c).

As shown in Fig. 4(a), the single capacitive loop was related to the electric double-layer capacitor, the diameter was approximately equal to the charge transfer resistance. The phase angle plots in Fig. 4(d) exhibited a characteristic of one time constant. Its chemical and electrochemical behavior model and equivalent circuit were displayed in Figs. 5(a) and Fig. 5(c). As shown in Fig. 5(a), there was no inhibitor film or an inhibitor film with a very low surface coverage owing to the low inhibitor concentrations (0.1-0.5 $\text{g}\cdot\text{L}^{-1}$)[45,50]. The aggressive ions enriched at the double electrode layer interface. Its electrochemical behavior could be expressed as a resistance and a capacitor in parallel connection presented in Fig. 5(c), where R_s was solution resistance, R_{ct} represented charge transfer resistance, Q_{dl} was electrical double-layer capacitor instead of ideal capacitor due to the roughness of the work electrode surface. For the two capacitive loops, the loop at high frequency range was associated to the behavior at electrode/electrolyte interface. The loop at middle and low frequency range was the behaviors at inhibitor film/electrolyte interface with a Warburg diffusion. With the increasing concentration of L-Arg, the thickness of inhibitor film and surface coverage of electrode surface increased. The diffusion of aggressive ions became increasingly difficult while they penetrated through the inhibitor film/inhibitor film micropores, and then, only few parts of aggressive ions reached the

electrode/electrolyte interface, which was approximatively considered as a semi-infinite diffusion model[51]. Their electrochemical behaviors were fitted to Figs. 5(b) and 5(d). Where R_f represented inhibitor film resistance, Q_f was film capacitor, W represented Warburg impedance. Moreover, it was clear from Fig. 4(d) that the Bode-Phase angle plots of these samples showed the characteristic of two time constants. Consequently, the high concentration (3.0-10.0 $\text{g}\cdot\text{L}^{-1}$) contributed to the increase of corrosion inhibition.

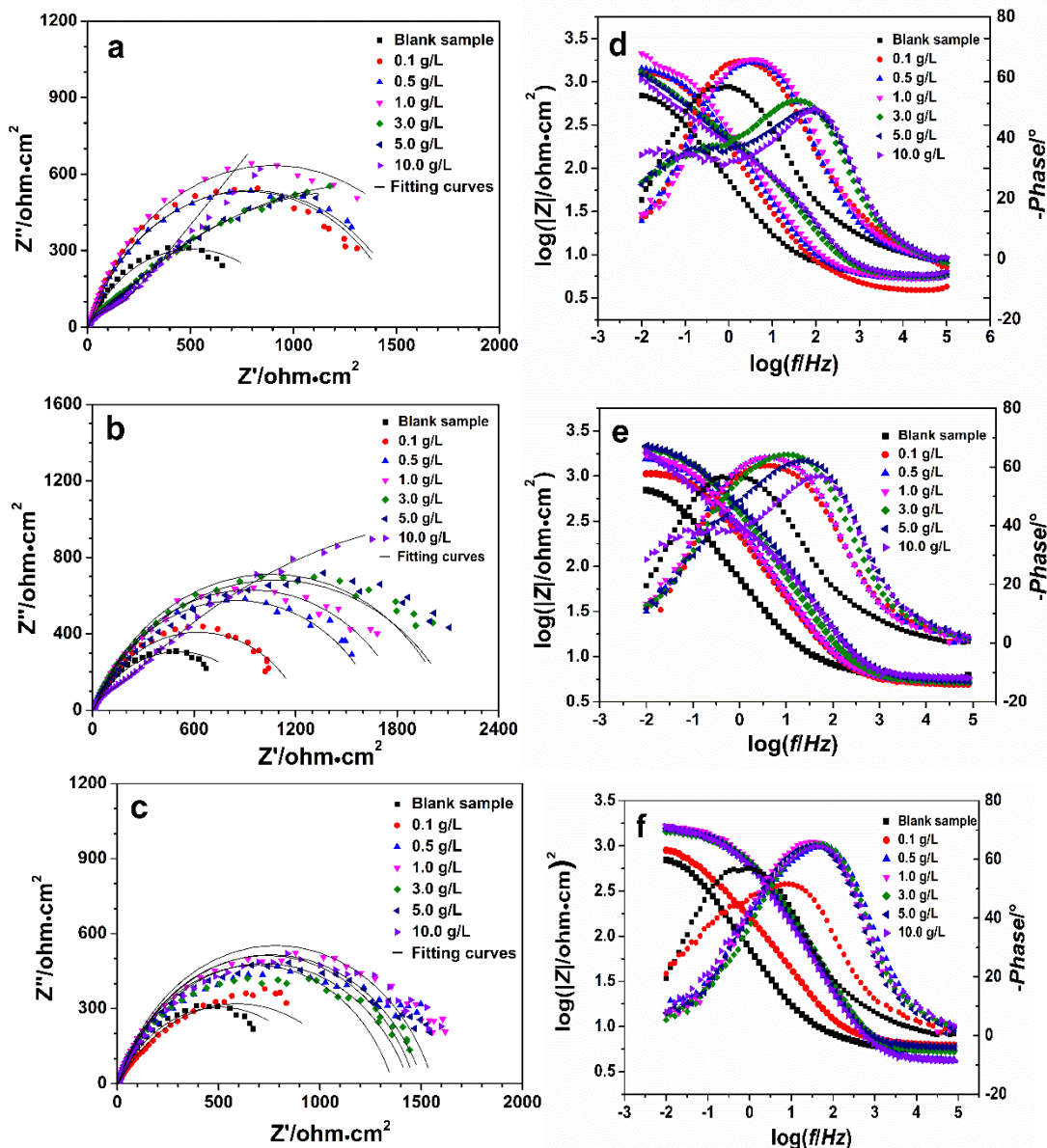


Figure 4. Nyquist and Bode plots of mild steel electrodes in presence of amino acids with various concentrations at 25 °C in 3.5% NaCl solution. (a) and (d) L-Arg, (b) and (e) L-Lys, (c) and (f) L-His.

From the Nyquist plots in Fig. 4(b), the diameter of the circle increased at the concentration range from 0.1 to 5.0 $\text{g}\cdot\text{L}^{-1}$, their Bode plots in Fig. 4(e) consisted of one time constant. Similarly, a Warburg impedance occurred at the inhibitor concentration of 10.0 $\text{g}\cdot\text{L}^{-1}$ and Bode plots presented a two time

constants. The corrosion inhibition mechanism was in accord with L-Arg. In the case of L-His, the diameter of capacitive loops did not change notably with the increasing concentration except for $0.1 \text{ g}\cdot\text{L}^{-1}$. All of the Bode plots showed one time constant.

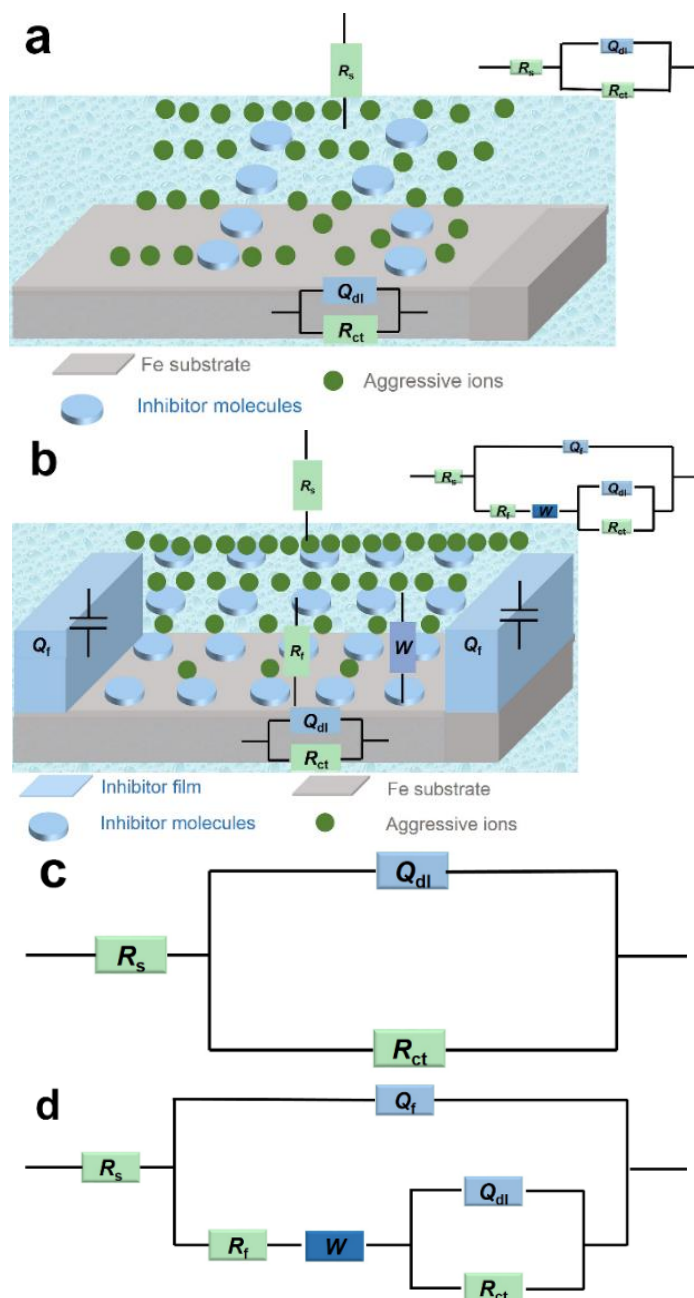


Figure 5. The mild steel surface in describing the chemical/physical characteristics of three amino acids (a) and (b) and equivalent circuits (c) and (d) for fitting the Nyquist diagrams.

The electrical equivalent circuits of the electrochemical process were exhibited in Figs. 5(c) and 5(d). The electrochemical parameters without and with various concentrations of amino acids L-Arg, L-Lys, L-His were fitted by using the software ZsimpWin and listed in Table 3. Thereof, the impedance of the *CPE* was expressed as[52]:

$$Z_{CPE} = \frac{1}{Y_0(j\omega)^n} \quad (10)$$

Where Y_0 ($\mu\Omega^{-1}\cdot\text{cm}^{-2}\cdot\text{s}^n$) represented *CPE* constant, j^2 was equal to -1, and ω was the angular frequency. n was corresponded to the metal surface state and a purely capacitive line on the complex plane plots. For $n = 1, 0.5$ and -1 , the *CPE* was equivalent to the pure capacitance component, Warburg impedance, and inductance, respectively. The inhibition efficiency (η) could obtain from the following equations:

$$\eta(\%) = \frac{R_{ct} - R'_{ct}}{R_{ct}} \times 100 \quad (11)$$

Here, R_{ct} and R'_{ct} represented the charge transfer resistance with and without inhibitors.

As was seen in Table 4, the R_{ct} and η increased during the lower concentrations for the samples with L-Arg and L-Lys. No appreciable change appeared at higher concentrations for L-Arg and L-Lys and L-His with all the concentrations except $0.1 \text{ g}\cdot\text{L}^{-1}$. The inhibition efficiency values obtained from EIS were in good accordance with the potentiodynamic polarization method.

Table 4. Electrochemical impedance parameters for the corrosion of mild steel in 3.5% NaCl solution containing various concentrations of amino acids at 25 °C.

Inhibitor	C ($\text{g}\cdot\text{L}^{-1}$)	R_s ($\Omega\cdot\text{cm}^2$)	R_f ($\Omega\cdot\text{cm}^2$)	Q_f		R_{ct} ($\Omega\cdot\text{cm}^2$)	Q_{dl}		W ($\mu\Omega^{-1}\cdot\text{cm}^{-2}\cdot\text{s}^{0.5}$)	η (%)
				Y_0 ($\mu\Omega^{-1}\cdot\text{cm}^{-2}\cdot\text{s}^n$)	n		Y_0 ($\mu\Omega^{-1}\cdot\text{cm}^{-2}\cdot\text{s}^n$)	n		
Blank	—	5.59	—	—	—	685	348.4	0.72	—	—
	0.1	5.94	—	—	—	1443	199.5	0.76	—	52.5
	0.5	5.76	—	—	—	1555	194.3	0.78	—	55.9
L-Arg	1.0	5.43	—	—	—	1778	186.1	0.78	—	61.4
	3.0	5.56	101.2	84.4	0.89	1962	171.2	0.80	250.0	65.1
	5.0	5.74	106.6	83.2	0.90	2034	169.1	0.82	243.2	66.3
	10.0	5.99	115.4	80.6	0.91	2218	160.4	0.82	235.5	69.1
	0.1	5.34	—	—	—	1141	213.6	0.74	—	40.0
L-Lys	0.5	5.33	—	—	—	1855	179.3	0.76	—	63.1
	1.0	5.35	—	—	—	1972	170.2	0.76	—	65.3
	3.0	5.30	—	—	—	2522	150.4	0.76	—	72.8
	5.0	5.47	—	—	—	2646	147.1	0.72	—	74.1
	10.0	5.85	122.9	72.4	0.90	2520	154.5	0.70	229.8	72.7
L-His	0.1	5.28	—	—	—	1467	177.2	0.63	—	53.3
	0.5	5.25	—	—	—	1944	172.8	0.75	—	64.7
	1.0	5.81	—	—	—	1956	170.4	0.77	—	65.0
	3.0	5.95	—	—	—	1899	174.8	0.74	—	63.9
	5.0	5.38	—	—	—	1964	171.1	0.77	—	65.1
	10.0	5.22	—	—	—	1980	169.6	0.75	—	65.4

3.3 Adsorption isotherm and thermodynamic adsorption parameters

The interactions between inhibitor molecules and electrode surface was studied by utilizing adsorption isotherm method. Two kinds of interactions exist between them. One was physisorption, which was the electrostatic interaction or intermolecular forces among the metal surface, anions/cations and molecules in the solution. The other was chemisorption, namely, the coordinate bond derived from the lone electron pair of nitrogen/oxygen atoms in amine/carboxyl groups and Fe-3d vacant

orbital[53,54]. Commonly, if the adsorbed layer is a monomolecular layer, there is a correlation between the inhibitor concentration (C) and the surface coverage (θ). Langmuir model can be used to express this correlation [55]. The mathematics formula was listed as follow:

$$\text{Langmuir isotherm: } \frac{\theta}{1-\theta} = K_{\text{ads}}C \quad (12)$$

Where K_{ads} was the adsorption equilibrium constant. The correlation coefficients (R^2) was used to choose the type of isotherm. The isotherm was presented in Fig. 6. The corresponding correlation coefficient was summarized in Table 5.

Table 5. Correlation coefficient (R^2) fitted from different isotherms.

Inhibitor	Correlation coefficient	
	R^2_{Langmuir}	
L-arginine	0.99	
L-lysine	0.99	
L-histidine	0.99	

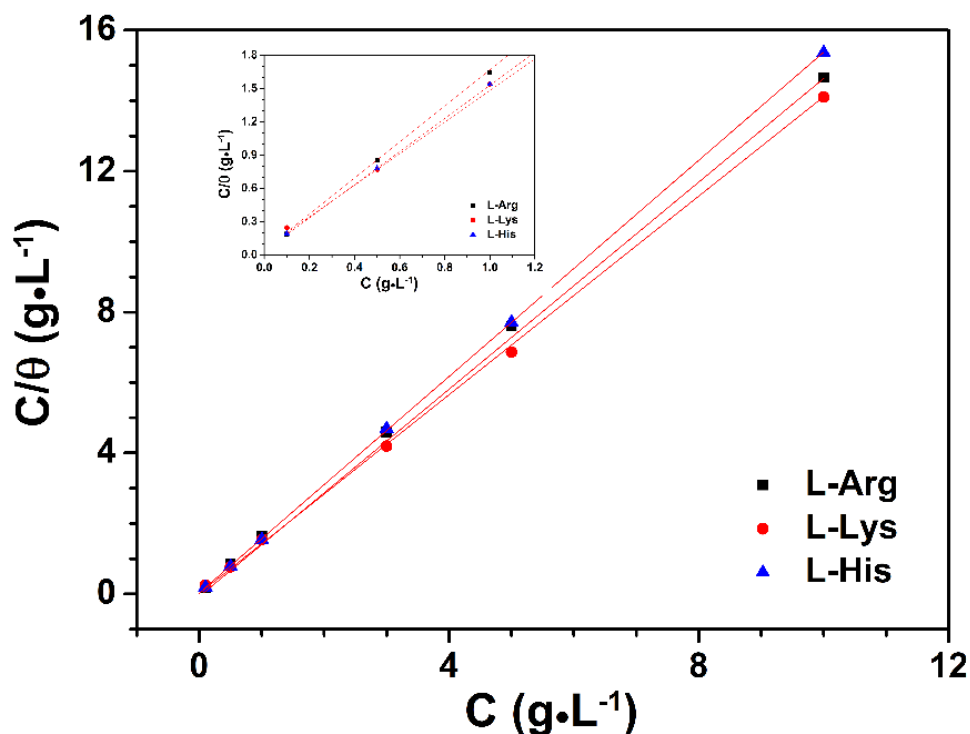


Figure 6. Fig. 6 Langmuir absorption isotherm for mild steel in 3.5% NaCl solution at 313K.

From Fig. 6 and Table 4 we could obtain the result from weight loss test that the absorption of three amino acids on mild steel surface obeyed the Langmuir isotherm. The value of K_{ads} was related to the Gibbs free energy ΔG_{ads} , which can be expressed using the equation as follows[56]:

$$\Delta G_{\text{ads}} = -RT \ln(55.5 \times K_{\text{ads}} \times 1000) \quad (13)$$

R was ideal gas constant, T was adsorption temperature (313 K), the calculated ΔG_{ads} and K values were illustrated in Table 5. In thermodynamics, the value of ΔG_{ads} around or higher than $-20 \text{ kJ}\cdot\text{mol}^{-1}$ is known as physisorption, whereas the chemisorption results in a more negative value of $-40 \text{ kJ}\cdot\text{mol}^{-1}$ and mixed adsorption was associated with the value range from $-20 \text{ kJ}\cdot\text{mol}^{-1}$ to $40 \text{ kJ}\cdot\text{mol}^{-1}$. In this case, the calculated ΔG_{ads} values were all around $-33 \text{ kJ}\cdot\text{mol}^{-1}$, indicated the adsorption process was a spontaneous reaction[56]. The inhibition mechanism was corresponded to mixed adsorption.

Table 6. Table 6 Equilibrium constant and Gibbs free energy of adsorption of mild steel in 3.5% NaCl with corrosion inhibitor of various concentrations at 25 °C.

Inhibitor	$K_{\text{ads}} (10^3 \text{ M}^{-1})$	$\Delta G_{\text{ads}} (\text{kJ}\cdot\text{mol}^{-1})$
L-arginine	6.32	-31.63
L-lysine	7.01	-31.89
L-histidine	6.64	-31.76

3.4 Corrosion inhibition mechanism of three amino acids

Commonly, the corrosion inhibition mechanism of organic inhibitors was the adsorption of inhibitor molecules on the metal surface. At this point, we could put forward the corrosion inhibition mechanism of three amino acids. According to the experiment results above, these three amino acids were all the mixed-type inhibitors, which included both physisorption and chemisorption. The schematic diagrams were illustrated in Fig. 7.

Fig. 7(a) showed the adsorption mechanism of L-Arg and L-Lys. The pH of 3.5 wt.% NaCl solution was about 8.0, which was less than pI of L-Arg (pI=10.76) and L-Lys (pI=9.74). Thus, the amino acid molecules would combine with the hydrogen ions and be positive charged particles. Several reactions existed in the solution as follows: R represented L-Arg and L-Lys.



As the equations mentioned above, the formation of R^+ led to the excess amount of hydroxyl ions in the solution, which would probably suppress the cathodic reaction shown as equation Eq (18), confirming the results of potentiodynamic polarization. In addition, the physisorption might occur as electrostatic attraction through the amino acid positive ions and chloride ions[33]. On the other hand, the chemisorption was the interaction between the lone electron pair in the inhibitor molecules and unoccupied orbital of iron atoms. The adsorption sites increased with the inhibitor concentration increased, the inhibition efficiency (η) increased until up to the state of saturation adsorption. At this moment, the value of inhibition efficiency showed little change.

Fig. 7(b) was the adsorption mechanism of L-His. Due to the less pI value (pI=7.59) versus pH, the L-His molecules were negative charged, resulting in the competitive adsorption with chloride ions

and a weaker electrostatic attraction. However, another physisorption between delocalized π bond in imidazole ring of L-His and Fe-3d appeared as a feedback bond (Fig. 7(c)). Chemisorption was also comprised of the coordinate bond[57]. The inhibition efficiency changed little with the increasing inhibitor concentration attributed to the nearly saturated adsorption at the low concentration of L-His.

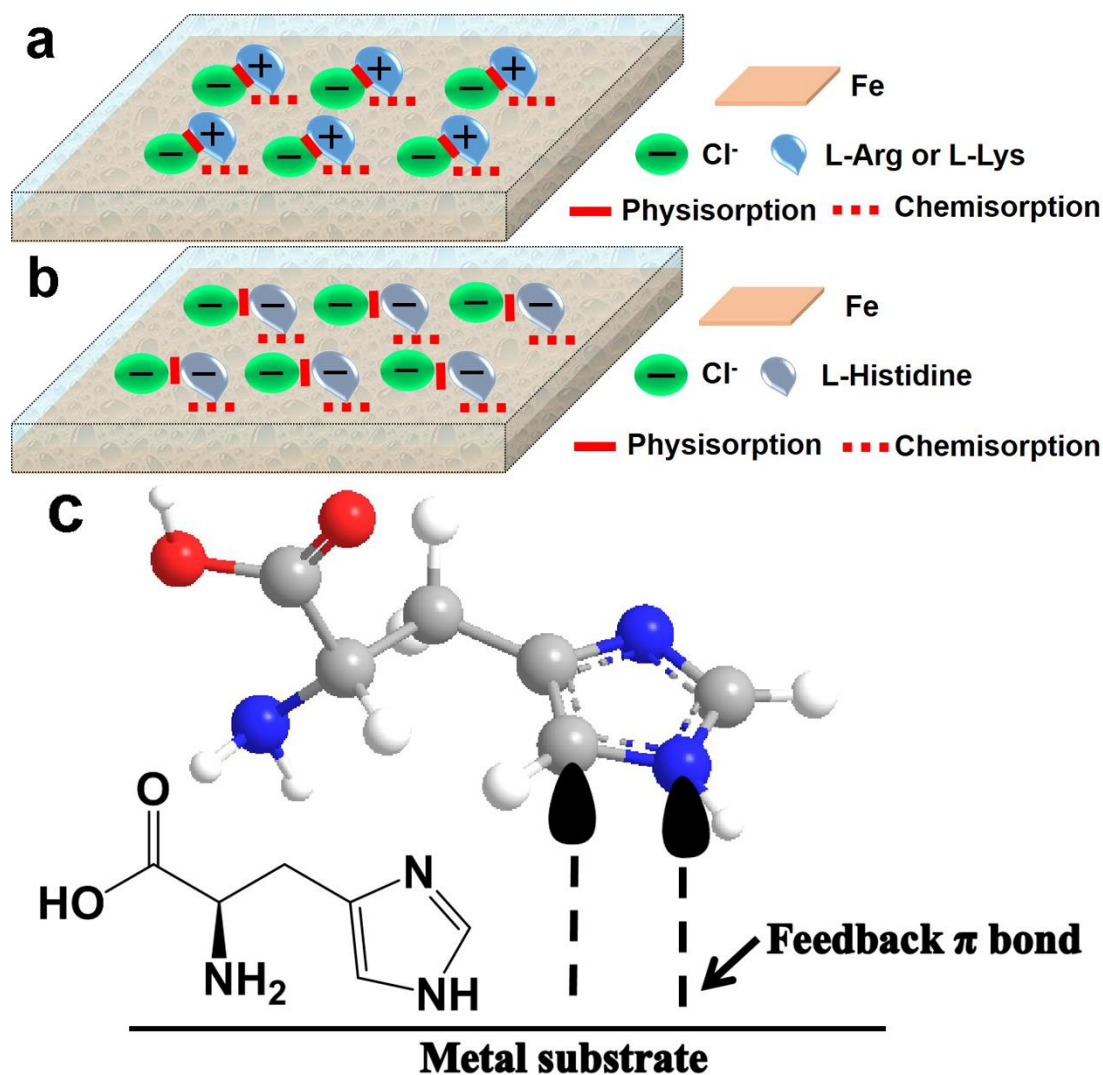


Figure 7. Schematic diagram of adsorption mechanism of three amino acids for mild steel in 3.5% NaCl solution, (a) L-Arg and L-Lys (b) L-His (c) Feedback π bond in L-His.

3.4 Scanning electron microscopy (SEM) observation

The SEM images of the mild steel substrate after immersion time in 3.5 wt.% NaCl solution in the absence and presence of three amino acids with the concentration of $1.0 \text{ g}\cdot\text{L}^{-1}$ and $10.0 \text{ g}\cdot\text{L}^{-1}$ were presented in Fig. 8. Fig. 8(a) showed an image of blank sample before immersion, and Fig. 8b showed the image of blank sample after immersion. It can be seen that the mild steel surface was severely attacked by NaCl solution, showing an irregular surface.

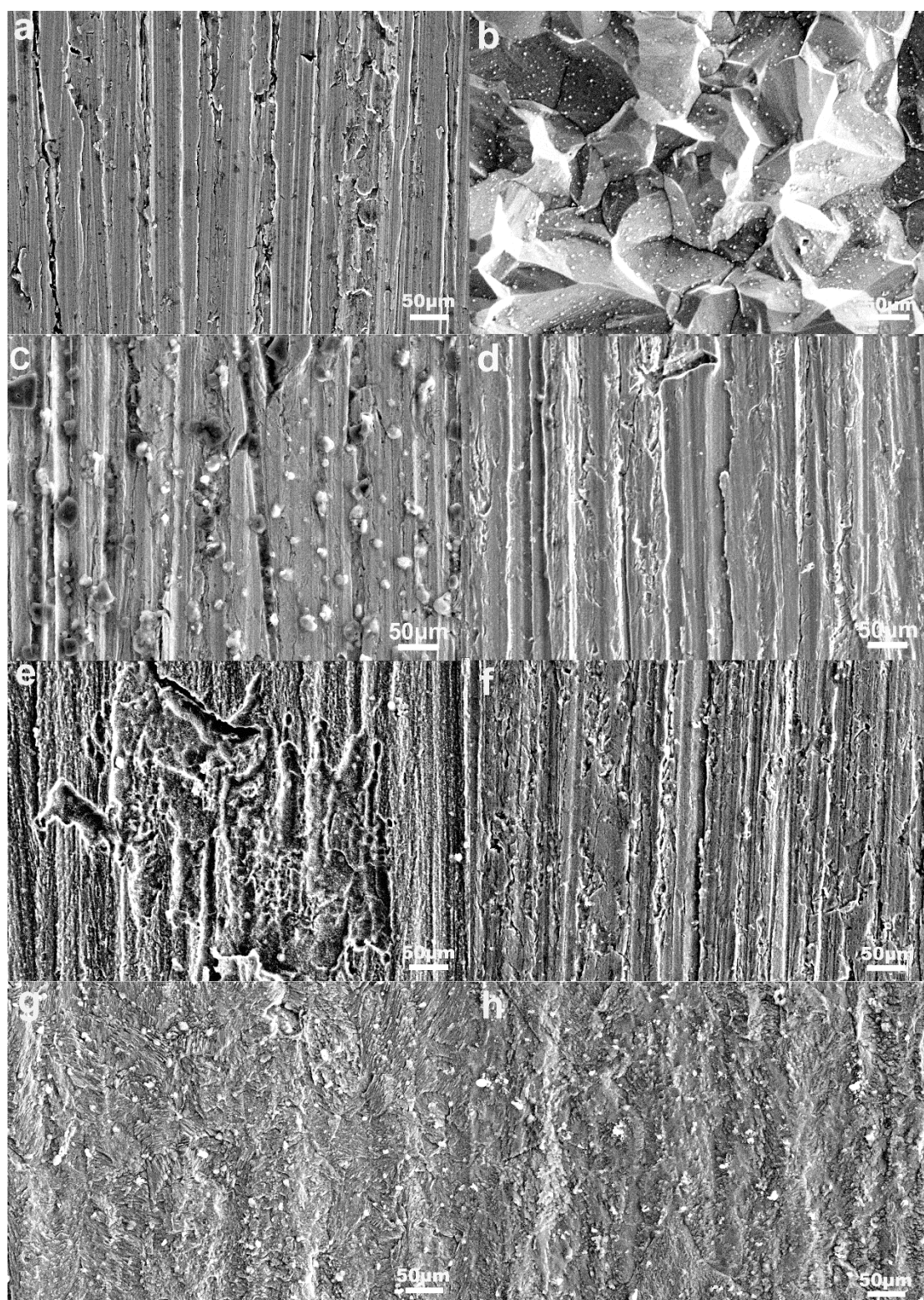


Figure 8. SEM images for (a) unexposed mild steel (b) exposed mild steel in blank solution and exposed mild steel in 3.5% NaCl containing L-Arg (c) $1.0 \text{ g}\cdot\text{L}^{-1}$ (d) $10.0 \text{ g}\cdot\text{L}^{-1}$, L-Lys (e) $1.0 \text{ g}\cdot\text{L}^{-1}$ (f) $10.0 \text{ g}\cdot\text{L}^{-1}$, and L-His (g) $1.0 \text{ g}\cdot\text{L}^{-1}$ (h) $10.0 \text{ g}\cdot\text{L}^{-1}$ at 25°C .

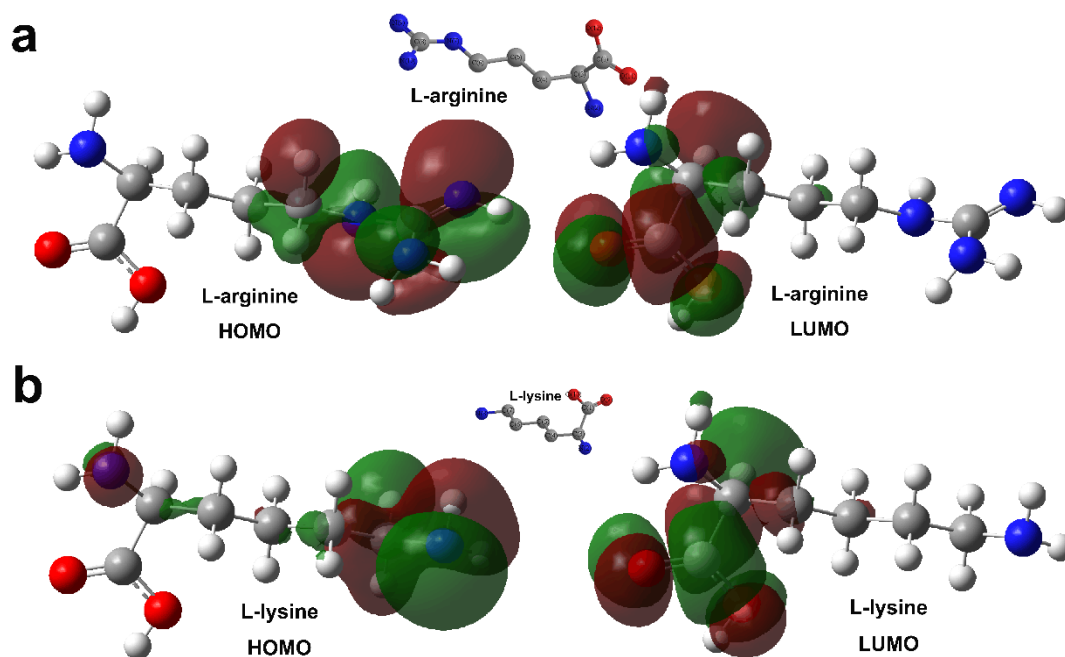
While the presence of three amino acids obviously reduced the corrosion rate and protected the metal from further corrosion (Figs. 8(c)-8(h)). In Figs. 8(c)-8(f), the presence of L-Arg and L-Lys with

increasing concentration showed less damage compared with the blank sample (Fig. 8(b)). Only slight corrosion was seen in the sample in the presence of $10.0 \text{ g}\cdot\text{L}^{-1}$ L-Arg and L-Lys. On the other hand, the corrosion state of sample with $1.0 \text{ g}\cdot\text{L}^{-1}$ L-His in Fig. 8g was similar with that in Fig. 8h, indicating the SEM results supported the weight loss and electrochemical results.

3.5. Quantum chemical calculation and molecular dynamics simulation

3.5.1 Quantum chemical calculation

Fig. 9 showed the geometry optimization of studied inhibitor molecule structures and their electron density isosurfaces of the highest occupied atomic orbital (HOMO) and lowest unoccupied molecular orbital (LUMO). Figs. 9(a) and 9(b) suggested that the electron distribution of HOMO of L-Arg and L-Lys was around atoms C-8, N-7, N-9, N-10 and C-7, N-8, respectively. And the activities of LUMO were both around the -COOH groups. The electron density was distributed around the atoms N-2, O-10, O-11 while it was distributed over the entire L-His molecule of LUMO owing to its conjugated structure of imidazole ring[38]. The HOMO indicates the ability of the rich electron sites in a molecule to donate electrons to the appropriate orbital of acceptor. Conversely, LUMO provides the electron deficiency region of a molecule, which suggests the ability of molecules to accept electrons from a donor. Therefore, nitrogen atoms in L-Arg and L-Lys and oxygen atoms has the better opportunity to donate electrons to metal surface.



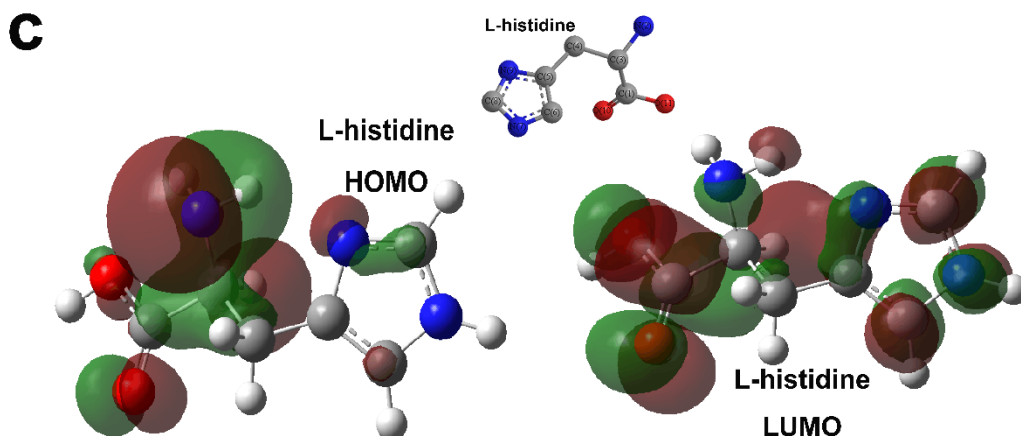


Figure 9. Electron density distributions on three amino acids (a) L- arginine HOMO and LUMO (b)L- Lys HOMO and LUMO (c)L-His HOMO and LUMO.

According to the Ref. [34,33,58], lower values of ΔE and γ , higher values of χ and ΔN of a corrosion inhibitor molecule may probably reflect the better inhibition efficiency. The quantum chemistry parameters were listed in Tables 7 and 8. As the results shown in weight loss parts foregoing, the highest inhibition efficiency of three amino acids was close to each other (10.0 g•L⁻¹, 64.2% 69.1% and 63%). The calculated values of these parameters showed a good correlation with the experimental results except for the trend in the ΔN , which might be interpreted as the π -electron conjugated structure in the L-His. This could lead to a higher E_{LUMO} value due to its electron density homogenization.

Table 7. Molecular orbital energies and dipole moments of L-Arg, L-Lys and L-His.

Inhibitor	E_{HOMO} (eV)	E_{LUMO} (eV)	ΔE (eV)	μ (D)
L-arginine	-6.246	0.141	6.387	4.888
L-lysine	-6.263	0.122	6.385	4.955
L-histidine	-6.207	0.224	6.431	4.639

Table 8. Quantum chemical descriptors of the three inhibitors calculated at B3LYP/6-31G(d,p) level of theory.

Inhibitor	I (eV)	A (eV)	χ (eV)	γ (eV)	ΔN
L-arginine	6.246	-0.141	3.053	3.194	0.618
L-lysine	6.263	-0.122	3.071	3.193	0.615
L-histidine	6.207	-0.224	2.992	3.216	0.622

The Fukui functions was used to certify the correctness of HOMO and LUMO. The local selectivity (active sites on the molecule) of three amino acids were studied by using the natural population analysis. The higher value of f_k^+ represented the atom or region which preferred to nucleophilic attack. Conversely, the higher value of f_k^- was a sign of the atom or region for electrophilic

attack[47]. The corresponding parameters were exhibited in Table 9. The corresponding molecule structures and atom sequence numbers were shown in Fig. 10. It was noticed that the highest value of f_k^+ in the molecules L-Arg and L-Lys concentrated on the nitrogen atoms and f_k^- around the oxygen atoms, respectively. With regard to L-His, the higher values of f_k^+ distributed in N-2 and carboxyl group, while f_k^- distributed over nearly the entire molecule, which suggested the carboxyl group might be the favorite site for both nucleophilic and electrophilic attacks. The results were agreed with the HOMO and LUMO analysis.

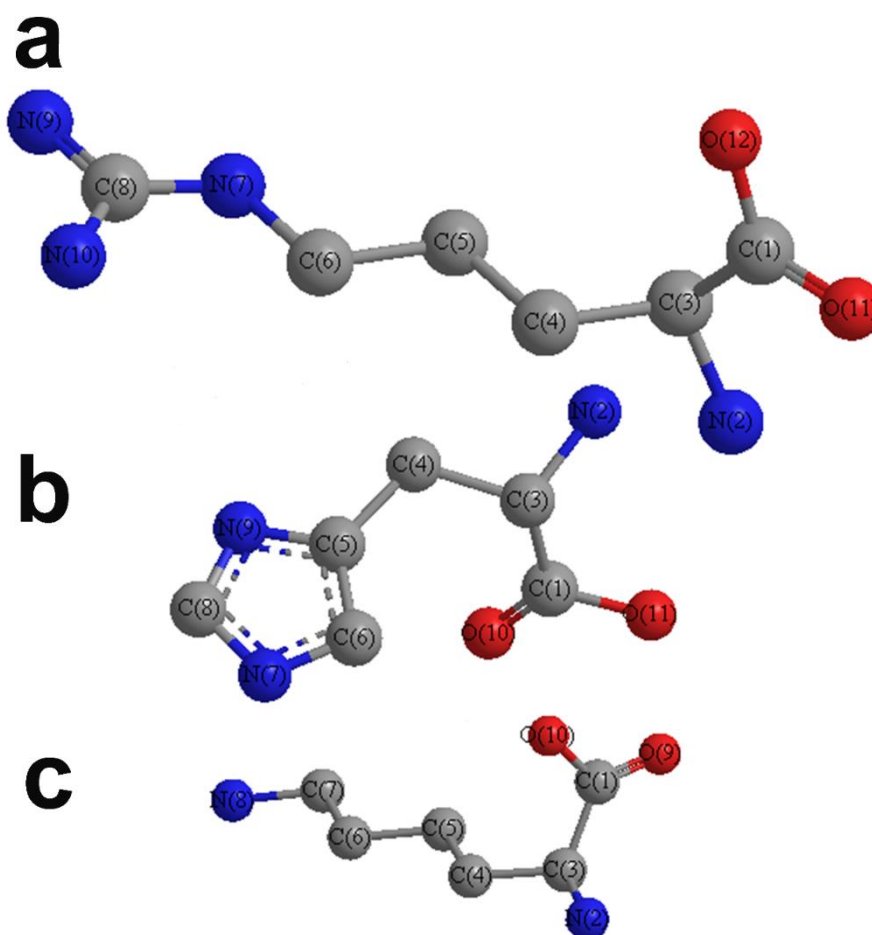


Figure 10. The optimal structures of (a) L-Arg (b) L-Lys (c) L-His.

Table 9. Pertinent natural population, Mulliken atom charges and Fukui functions of the three inhibitors calculated at B3LYP/6-31G(d,p).

Inhibitor	Atoms	$P(N+1)$	$P(N)$	$P(N-1)$	f_k^+	f_k^-
L-arginine	N (2)	-0.498	-0.607	-0.605	0.109	-0.002
	N (7)	-0.448	-0.549	-0.530	0.101	-0.019
	N (9)	-0.438	-0.667	-0.638	0.229	-0.029

	N (10)	-0.570	-0.654	-0.592	0.084	-0.062
	O (11)	-0.432	-0.460	-0.609	0.028	0.149
	O (12)	-0.480	-0.473	-0.534	-0.007	0.061
L-lysine	N (2)	-0.442	-0.606	-0.600	0.164	-0.006
	N (8)	-0.444	-0.608	-0.575	0.164	-0.033
	O (9)	-0.426	-0.464	-0.631	0.038	0.167
	O (10)	-0.470	-0.471	-0.545	0.001	0.074
L-histidine	C (1)	0.641	0.579	0.476	0.062	0.103
	N (2)	-0.473	-0.586	-0.616	0.113	0.003
	C (3)	-0.069	-0.008	0.012	-0.061	-0.020
	C (4)	-0.246	-0.234	-0.200	-0.012	-0.034
	C (5)	0.233	0.207	0.210	0.026	-0.003
	C (6)	0.139	0.066	-0.038	0.073	0.104
	N (7)	-0.487	-0.527	-0.512	0.040	-0.015
	C (8)	0.357	0.265	0.184	0.092	0.081
	N (9)	-0.482	-0.482	-0.528	0	0.046
	O (10)	-0.397	-0.475	-0.585	0.078	0.110
	O (11)	-0.475	-0.475	-0.542	0	0.067

3.5.2 Molecular dynamic simulation

Molecular dynamic simulation provided more insight into the adsorption process on Fe surface of inhibitor molecules. The adsorption configurations of (a) L-Arg, (b) L-Lys, (c) L-His on Fe (110) surface was simulated and the simulation results were illustrated in Fig. 11.

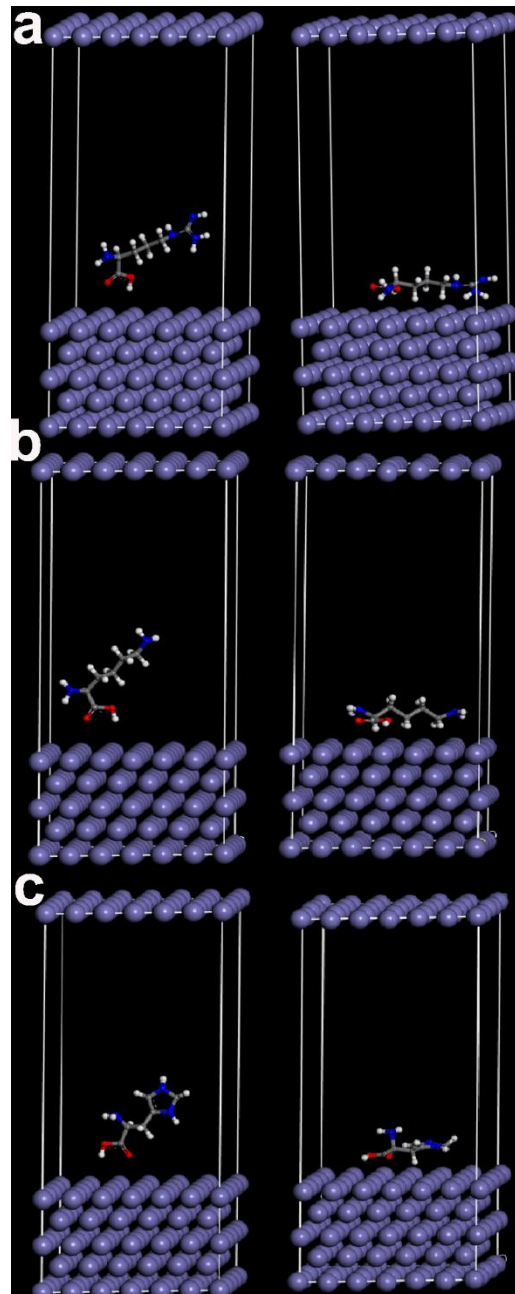


Figure 11. Most stable low energy configuration for the adsorption of (a)L-Arg (b) L-Lys (c) L-His on Fe (110) surface from material studios.

The minimum distance between the three amino acid molecules and Fe (110) surface was 2.313, 2.349 and 2.448 nm, respectively. This was the evidence that the three amino acids could adsorb on Fe surface through nitrogen and oxygen atoms. The corresponding parameters such as total energy (E_{total}), inhibitor energy ($E_{\text{inhibitor}}$), surface energy (E_{surface}), interaction energy ($E_{\text{interaction}}$) and binding energy (E_{binding}) were exhibited in Table 10. The value of E_{binding} was calculated by using the equations as follows[34]:

$$E_{\text{interaction}} = E_{\text{total}} - (E_{\text{inhibitor}} + E_{\text{surface}})$$

$$E_{\text{binding}} = -E_{\text{interaction}}$$

The absorption capacity between the inhibitor molecules and Fe surface could be measured by the value of binding energy. Where the higher E_{binding} value is, the stronger adsorption capacity of inhibitor molecule is[47]. As the result in Table 10, the more positive values of E_{binding} attributed to the stronger adsorption showed the E_{binding} values obeyed the sequence of L-Lys > L-Arg > L-His, which was in good consistent with the quantum chemistry calculation and experiments results.

Table 10. Molecular dynamic simulation energies of the three amino acids on Fe (110) surface (in $\text{KJ}\cdot\text{mol}^{-1}$)

Inhibitor	E_{total}	$E_{\text{inhibitor}}$	E_{surface}	$E_{\text{interaction}}$	E_{binding}
L-arginine	-1308.4	-10.4	-1276.3	-21.7	21.7
L-lysine	-1283.3	-15.2	-1276.3	-22.2	22.2
L-histidine	-1289.9	-6.5	-1276.3	-20.1	20.1

4. CONCLUSION

In summary, the corrosion inhibition performances of L-arginine (L-Arg), L-lysine (L-Lys) and L-histidine (L-His) were investigated in this work. The inhibition capacity of three amino acids were determined by electrochemical, weight loss, quantum chemistry calculation and molecular dynamic simulation techniques. The adsorption mechanism was proposed to interpret corrosion inhibition properties. The following conclusions were given from our studies.

(1) From the electrochemical experiments and weight loss measurements, the three amino acids exhibited mixed-type corrosion inhibitors. The inhibition efficiency of L-Arg and L-Lys increased with the increase in the concentration and reached the maximum value of 74.1% and 69.1%, respectively. There was no specific change trend in corrosion efficiency of L-His with the increase in the concentration.

(2) The adsorption behaviors of three amino acids obeyed Langmuir isotherm. Adsorption mechanisms of L-Arg and L-Lys included both the chemisorption derived from the coordinate bond provided by nitrogen or oxygen atoms and Fe-3d empty orbitals and the physisorption attributed to the electrostatic interaction between protonated amino acid molecules and Cl^- . The mechanism of L-His was the chemisorption which contained coordinate bond and π -back-donation bond.

(3) The quantum chemistry calculation including the front orbital energy and Fukui function analysis and molecular dynamics simulation results gave more insight into the corrosion inhibition mechanism at molecular level, which was in good accord with the experimental results.

ACKNOWLEDGEMENTS

The authors gratefully acknowledge financial support by Doctor foundation of Qingdao University of Science and Technology (No. 010022894).

References

1. R. Barker, B. Pickles and T. L. Hughes, *Electrochim Acta*, 338 (2020) 1385-1402.
2. G. Sigircik, T. Tuken and M. Erbil, *Appl. Surf. Sci.*, 324 (2015) 232-239.
3. R. Solmaz, *Corros. Sci.* 81 (2014) 75-84.
4. R. Yildiz, *Corros.Sci.*, 90 (2015) 544-553.
5. A.S. Fouda and A.S. Ellithy, *Corros.Sci.*, 51 (2009) 868-875.
6. A. Doner, E.A. Sahin, G. Kardas and O. *Corros.Sci.*, 66 (2013) 278-284.
7. P. Singh, M. Makowska-Janusik, P. Slovensky and M.A. Quraishi, *J. Mol. Liq.*, 220 (2016) 71-81.
8. H. Ashassi-Sorkhabi, M.R. Majidi and K. *Appl.Surf. Sci.*, 225 (2004) 176-185.
9. A.M. Fekry and R.R. Mohamed, *Electrochim Acta*, 55 (2010) 1933-1939.
10. E.E. Oguzie, *Mater. Lett.*, 59 (2005) 1076-1079.
11. A.V. Shanbhag, T.V. Venkatesha, R.A. Prabhu, R.G. Kalkhambkar and G.M. Kulkarni, *J. Appl. Electrochem.*, 38 (2007) 279-287.
12. M. Bobina, A. Kellenberger, J.-P. Millet, C. Muntean and N. Vaszilcsin, *Corros.Sci.*, 69 (2013) 389-395.
13. R. Yildiz, A. Doner, T. Dogan and I. Dehri, *Corros.Sci.*, 82 (2014) 125-132.
14. H. Bentrach, Y. Rahali, A. Chala, *Corros.Sci.*, 82 (2014) 426-431.
15. B.D. Mert, M. Erman Mert, G. Kardas and B. Yazici, *Corros.Sci.*, 53 (2011) 4265-4272.
16. P. Mourya, P. Singh, A.K. Tewari, R.B. Rastogi and M.M. Singh, *Corros.Sci.*, 95 (2015) 71-87.
17. A. Yurt, A. Balaban, S.U. Kandemir, G. Bereket and B. Erk, *Mater. Chem. Phys.*, 85 (2004) 420-426.
18. M. Ozcan, I. Dehri and M. Erbil, *Appl.Surf. Sci.*, 236 (2004) 155-164.
19. S.M. Tawfik and N.A. Negm, *J. Mol. Liq.*, 215 (2016) 185-196.
20. G. Hailiang, Z. Shengtao and X. Wang, *Int J Electrochem Sci.*, 8 (2019) 7842-7857.
21. S.A. Umoren, M.J. Banera, T. Alonso-Garcia, C.A. Gervasi, M.V. Mirifico, *Cellul.*, 20 (2013) 2529-2545.
22. Y. Sangeetha, S. Meenakshi and C.S. Sundaram, *Carbohydr. Polym.*, 136 (2016) 38-45.
23. M.N. El-Haddad, *Carbohydr. Polym.*, 112 (2014) 595-602.
24. T. Junlei and H. Yuxin, *Int J Electrochem Sci.*, 3 (2019) 2246-2264.
25. M. Yadav, T.K. Sarkar and T. Purkait, *J. Mol. Liq.*, 212 (2015) 731-738.
26. M.V. Fiori-Bimbi, P.E. Alvarez, H. Vaca and C.A. Gervasi, *Corros.Sci.*, 92 (2015) 192-199.
27. A. El Bribri, M. Tabyaoui, B. Tabyaoui, H. El Attari and F. Bentiss, *Mater. Chem. Phys.*, 141 (2013) 240-247.
28. M. Znini, L. Majidi, A. Bouyanzer, J. Paolini, J.M. Desjobert, J. Costa and B. Hammouti, *Arab. J. Chem.*, 5 (2012) 467-474.
29. N. Soltani, N. Tavakkoli, M. Khayat Kashani, A. Mosavizadeh, E.E. Oguzie and M.R. Jalali, *J. Ind. Eng. Chem.*, 20 (2014) 3217-3227.
30. K. Wan, P. Feng, B. Hou and Y. Li, *RSC Adv.*, 6 (2016) 77515-77524.
31. A.M. Al-Sabagh, N.M. Nasser, O.E. El-Azabawy and A.E.E. Tabey, *J. Mol. Liq.*, 219 (2016) 1078-1088.
32. M. Yadav, L. Gope and T.K. Sarkar, *Res. Chem. Intermediat.*, 42 (2016) 2641-2660.
33. M.A. Amin, K.F. Khaled, Q. Mohsen and H.A. Arida, *Corros.Sci.*, 52 (2010) 1684-1695.
34. Z. Cao, Y. Tang, H. Cang, J. Xu, G. Lu and W. Jing, *Corros.Sci.*, 83 (2014) 292-298.
35. S. Kaya, B. Tuzun, C. Kaya and I.B. Obot, *J. Taiwan Inst. Chem. E.*, 58 (2016) 528-535.
36. D. Turcio-Ortega, T. Pandiyan and J. Cruz, *J. Mol Struct.*, 16 (2019) 131-145.
37. S. Xia, M. Qiu, L. Yu, F. Liu and H. Zhao, *Corros.Sci.*, 50 (2008) 2021-2029.
38. L.M. Rodríguez-Valdez, W. Villamizar, M. Casales, J.G. Gonzalez-Rodriguez, A. Martínez-Villafane, L. Martinez and D. Glossman-Mitnik, *Corros.Sci.*, 48 (2006) 4053-4064.
39. Z. Moradi and M. Attar, *Appl.Surf. Sci.*, 317 (2014) 657-665.

40. R.G. Pearson, *Inorg. Chem.*, 27 (1988) 734-740.
41. X. Zheng, S. Zhang, M. Gong and W. Li, *Ind. Eng. Chem. Res.*, 53 (2014) 16349-16358.
42. S.K. Saha, A. Dutta, P. Ghosh, D. Sukul and P. Banerjee, *Phys. Chem. Chem. Phys.*, 17 (2015) 5679-5690.
43. E. Khamis, F. Bellucci, R. Latanision and E. El-Ashry, *Corros.*, 47 (1991) 677-686.
44. Y. Wei, K.F. Hsueh and G.W. Jang, *Polym.*, 35 (1994) 3572-3575.
45. S. Saker, N. Aliouane, H. Hammache, S. Chafaa and G. Bouet, *Ionics*, 21 (2015) 2079-2090.
46. H.M. Abd El-Lateef, M. Ismael and I. Mohamed, *Corros. Rev.*, 33 (2015) 77-97.
47. L.O. Olasunkanmi, I.B. Obot, M.M. Kabanda and E.E. Ebenso, *J. Phys. Chem. C*, 119 (2015) 16004-16019.
48. A.R. El-Sayed, H.S. Mohran and H.M. Abd El-Lateef, *Corros.Sci.*, 52 (2010) 1976-1984.
49. C. Cao, *Corros.Sci.*, 38 (1996) 2073-2082.
50. G. Golestani, M. Shahidi and D. Ghazanfari, *Appl.Surf. Sci.*, 308 (2014) 347-362.
51. H. Tian, Y.F. Cheng, W. Li and B. Hou, *Corros.Sci.*, 100 (2015) 341-352.
52. C. Hsu and F. Mansfeld, *Corros.*, 57 (2001) 747-748.
53. A.Y. Musa, R.T.T. Jalgham and A.B. Mohamad, *Corros.Sci.*, 56 (2012) 176-183.
54. X. Ma, X. Jiang, S. Xia, M. Shan, X. Li, L. Yu and Q. Tang, *Appl.Surf. Sci.*, 371 (2016) 248-257.
55. M. Bouklah, B. Hammouti, M. Lagrenee and F. Bentiss, *Corros.Sci.*, 48 (2006) 2831-2842.
56. J.M. Cases and F. Villieras, *Langmuir*, 8 (1992) 1251-1264.
57. S.H. Yoo, Y.W. Kim, K. Chung, N.K. Kim and J.S. Kim, *Ind. Eng. Chem. Res.*, 52 (2013) 10880-10889.
58. C. Verma, L.O. Olasunkanmi, E.E. Ebenso, M.A. Quraishi and I.B. Obot, *J. Phys. Chem. C*, 120 (2016) 11598-11611.

© 2020 The Authors. Published by ESG (www.electrochemsci.org). This article is an open access article distributed under the terms and conditions of the Creative Commons Attribution license (<http://creativecommons.org/licenses/by/4.0/>).